Tree Physiology 35, 305–318
doi:10.1093/treephys/tpv010

Research paper

Biophysical modelling of intra-ring variations in tracheid features and wood density of *Pinus pinaster* trees exposed to seasonal droughts

Sarah Wilkinson[1,2,3], Jérôme Ogée[1], Jean-Christophe Domec[1], Mark Rayment[2] and Lisa Wingate[1]

[1]INRA UMR 1391 ISPA Bordeaux Sciences Agro, 71 Avenue Edouard Bourleaux, 33140 Villenave d'Ornon, France; [2]School of the Environment, Natural Resources and Geography, Bangor University, Deiniol Road, Gwynedd LL57 2UW, UK; [3]Corresponding author (s.l.wilkinson@sms.ed.ac.uk)

Received July 3, 2014; accepted January 26, 2015; published online March 12, 2015; handling Editor Nathan Phillips

Process-based models that link seasonally varying environmental signals to morphological features within tree rings are essential tools to predict tree growth response and commercially important wood quality traits under future climate scenarios. This study evaluated model portrayal of radial growth and wood anatomy observations within a mature maritime pine (*Pinus pinaster* (L.) Aït.) stand exposed to seasonal droughts. Intra-annual variations in tracheid anatomy and wood density were identified through image analysis and X-ray densitometry on stem cores covering the growth period 1999–2010. A cambial growth model was integrated with modelled plant water status and sugar availability from the soil–plant–atmosphere transfer model MuSICA to generate estimates of cell number, cell volume, cell mass and wood density on a weekly time step. The model successfully predicted inter-annual variations in cell number, ring width and maximum wood density. The model was also able to predict the occurrence of special anatomical features such as intra-annual density fluctuations (IADFs) in growth rings. Since cell wall thickness remained surprisingly constant within and between growth rings, variations in wood density were primarily the result of variations in lumen diameter, both in the model and anatomical data. In the model, changes in plant water status were identified as the main driver of the IADFs through a direct effect on cell volume. The anatomy data also revealed that a trade-off existed between hydraulic safety and hydraulic efficiency. Although a simplified description of cambial physiology is presented, this integrated modelling approach shows potential value for identifying universal patterns of tree-ring growth and anatomical features over a broad climatic gradient.

Keywords: IADF, MuSICA, wood anatomy, wood formation.

Introduction

Tree radial growth patterns are controlled by the cambium, once dubbed the 'least understood plant meristem' (Fritts 1966). Despite on-going mechanistic ambiguity, cambial activity is known to be strongly influenced by plant carbon–water relations (Larson 1994, Savidge 2001) that affect hormone levels (e.g., auxin) and turgor pressure in the developing xylem cells of the cambium (Fritts 2001, Kramer 2001, Vaganov et al. 2006). Over a growing season, trees from regions with seasonal rainfall variations balance water demand and supply through xylem modification, often producing large 'earlywood' tracheids that maximize hydraulic efficiency and 'latewood' tracheids with narrower lumen and presumably thicker cell walls (Fritts 2001, Domec and Gartner 2002*a*, Tyree and Zimmermann 2002). Such fluctuations in the number, lumen size and wall thickness of cells produced by the cambium are imprinted in wood density profiles. Thus, tree-ring anatomical features and wood density profiles mirror temporal variations in environmental conditions; over what timescale, and to what extent, remains unclear.

Special anatomical features such as false rings, or more specifically intra-annual density fluctuations (IADFs), are widely documented in dendrochronological studies and their existence demonstrates that trees can exhibit rapid acclimation during wood formation. Intra-annual density fluctuations represent abrupt changes in the density profile that are highly co-ordinated with temporal variations in water availability (Wimmer et al. 2000, Rigling et al. 2001, 2002, Campelo et al. 2007). Drought events can trigger the formation of latewood-like cells within earlywood, so-called 'false rings', while earlywood-like cells may emerge in response to rainfall after the seasonal drought in late summer or early autumn and interrupt the formation of latewood (Fritts 2001, Bouriaud et al. 2005, Park et al. 2006). Rainfall events are well coupled to increased radial increment because higher whole-tree water availability generates positive turgor pressure within the cambial zone, driving irreversible cell enlargement (Lockhart 1965, Zweifel et al. 2006). Conversely, cambial function also reacts to water deficit within a matter of days, and cell enlargement becomes physically restricted by a reduction in turgor pressure (Schweingruber 1988), causing the cambium to produce smaller but also fewer cells (Abe and Nakai 1999, Abe et al. 2003). Campelo et al. (2007) presented the first study linking the position of the IADF within the ring to the time of the triggering factor during the growing season. Intra-annual density fluctuation morphology and radial position within the annual ring can therefore help identify periods of atypically low or high water availability (Rigling et al. 2001, Battipaglia et al. 2010) or other weather anomalies, for example, warm temperatures and a low water availability in spring followed by a wet October increased the probability of cambial reactivation and latewood IADFs occurring in stands of maritime pine in NW Spain (Rozas et al. 2011).

The fact that trees can exhibit rapid acclimation during wood formation is not surprising, given the pivotal role of xylem architecture in hydraulic function. Indeed water transport through the xylem is extremely vulnerable and must be maintained under drought conditions to avoid tissue damage and mortality (Sperry et al. 2008). Two mechanisms linked to cell wall thickness can engender discontinuity in the stem xylem water column. The first occurs when xylem pressure drops below the air-seeding threshold, enabling air bubbles to be pulled into adjacent conduits through pit membrane pores (Tyree and Sperry 1989). The second mode of failure involves sap tensions that implode xylem cells (Hacke et al. 2001). Xylem failure through air-seeding is affected by the morphology of bordered pits (Domec et al. 2006, Choat et al. 2008, Delzon et al. 2010), which is directly related to cell wall thickness (Domec et al. 2009), whereas xylem failure by implosion is determined by the ratio of cell wall thickness to lumen diameter (Hacke et al. 2001, Pittermann et al. 2006). Hence, the relative proportion and density of latewood may have a crucial role in hydraulic acclimation.

Intra-ring density profiles and climate data interpreted together could reveal the dynamic coupling between tree growth and weather variations (Rigling et al. 2001, 2002, De Micco et al. 2007, Battipaglia et al. 2010). However, there are a number of difficulties in assessing the extent of this biophysical relationship, particularly with regard to the temporal phasing of density measurements with climate data (Deleuze and Houllier 1998, Vaganov et al. 2006). Process-based photosynthesis and transpiration models that attempt to recreate cambial dynamics have the potential to resolve such limitations. These models can be used to predict xylem properties such as turgor pressure, hydraulic conductance, cell number and density under seasonally varying environmental conditions (Deleuze and Houllier 1998, Vaganov et al. 2006, Hölttä et al. 2010). This may help synchronize temporal climate patterns and profiles of wood density more closely, leading to improved understanding of the mechanisms behind intra-annual fluctuations.

Maritime pine—*Pinus pinaster* (L.) Aït.—is known to exhibit IADFs, especially in the latewood in response to autumn rain events (De Micco et al. 2007, Vieira et al. 2010, Rozas et al. 2011). This study aimed to integrate results from a cambial activity model and tree-ring data on *P. pinaster* from a recurrently droughted site in southern France. The process-based, soil–vegetation–atmosphere transfer model MuSICA (Ogée et al. 2003, 2009, Domec et al. 2012) was used to generate continuous estimates of soil water content, evapotranspiration and whole-tree non-structural carbohydrates (NSCs) from observed climate data. MuSICA outputs were then used to generate temporal and spatial variations in tracheid production and wood density over the same period, using the model proposed by Deleuze and Houllier (1998). Many complex aspects of cambial development are not included in this model. However, it provides a first attempt at linking environmental variations to the cambial environment and evaluating the impact of plant water status on wood growth and density. Therefore, this model was selected on the basis of providing the simplest solution to modelling cambial activity in accordance with the objectives of the study and was the most appropriate model based on our data set of input parameters. The ability of the combined models to predict wood density was investigated by comparing model outputs against observed wood density profiles obtained from both anatomical and X-ray densitometry measurements. Based on the hypothesis that IADFs occur in response to sudden changes in water availability, and play a critical role in the trade-off between hydraulic efficiency and hydraulic safety, we also investigated the ability of the model to predict the timing and extent of IADFs as well as changes in the hydraulic properties of the xylem, as deduced from anatomical observations.

Materials and methods

Study site

The study was conducted at Le Bray, an even-aged Maritime pine forest planted in 1970, located ~20 km south of Bordeaux,

France (44°43′N, 0°46′W, 62 m above sea level). In 2011, when this study was conducted, the mean tree height was 20 m and the tree density was ~300 stems per hectare. The climate is characterized by occasional strong winds and seasonal deficits in water availability: rainfall exceeds evapotranspiration during winter months, while drought afflicts summer and autumn growth. The mean cumulative precipitation of June and July is 99 mm and the mean air temperature is 19.6 °C, while the mean cumulative precipitation of September and October is 144 mm and the mean air temperature is 16.1 °C. Water table depth ranges between the soil surface and about −2 m. The topography is flat and prevents any surface run-off (Ogée et al. 2003).

Image analysis of tracheid features

For cell measurements, a single wood core (12 mm in diameter) was collected at breast height (1.3 m) from five dominant trees, wrapped in aluminium foil and stored at 5 °C within 2 h of sampling. To avoid compression wood, trees were cored from bark to pith along the azimuth of the prevailing wind direction. Cores were manually dated and cut into sections covering the years 1999–2010 when meteorological data were available. Transverse sections of 30 µm in thickness were cut with a sliding microtome, stained with 1% aqueous safranin-O and observed hydrated under a light microscope (Leica DM300, Heerbrugg, Switzerland). Digital images for each section were taken at ×4, ×100 and ×400 magnifications using a digital camera (Leica EC3) mounted on the microscope. Section images for each core at a ×100 magnification were then merged to obtain a single image of each ring. Intra-annual density fluctuations were defined as those formed in the middle of the latewood (IADF type L) and those formed at the end of the latewood (IADF type L+), according to the classification described by Campelo et al. (2007).

Tracheid radial dimensions were determined using the public-domain image analysis software (Image-J 136b; NIH, Bethesda, Maryland, USA). Lumen diameter, cell wall thickness and total cell number were measured along three radial files in each annual ring (Figure 1). A mean radial file for each ring was then calculated by normalizing the radial file by the minimum number of cells per ring and computing the relative cell number. Tracheid wood density ($\rho_{tracheid}$, the density of the wood with tracheids only and no live tissue) was then estimated from the anatomical data assuming that the mass of the lumen is negligible compared with the mass of the cell walls:

$$\rho_{tracheid} = \rho_{cw} \frac{A_{cw}}{A_{cw} + A_L} \quad (1)$$

where ρ_{cw} (kg dm^{-3}) denotes cell wall density, and A_{cw} and A_L (m^2) denote the surface area of the cell wall and lumen of the tracheids, respectively. For square-shape tracheids, these surface areas can be easily deduced from observations of lumen radial diameter L (m) and cell wall thickness w (m). However, tracheid geometry varied along the radial profile with both rectangular and hexagonal shapes being predominant (Figure 1). Since no significant difference was found between those two geometrical shapes ($P = 0.978$), tracheid wood density was in

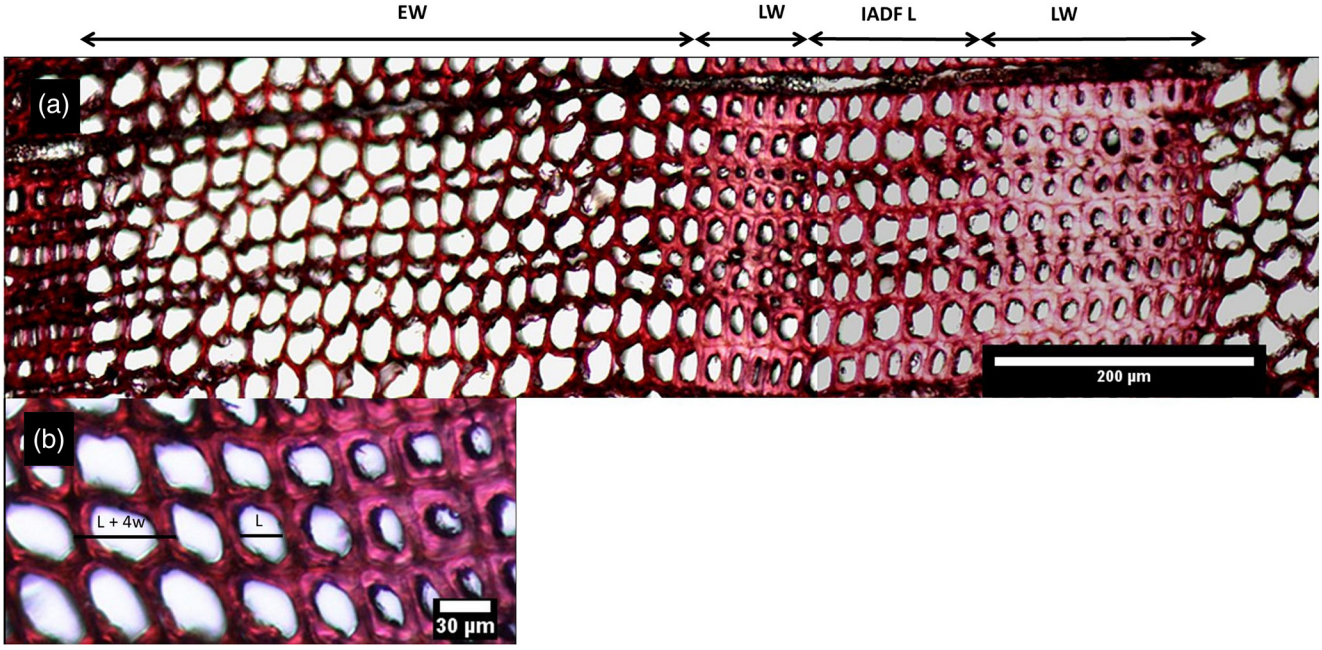

Figure 1. Light microscope images showing (a) the 2002 growth ring with the anatomical differentiation of earlywood cells (EW), the earlywood/latewood transition (LW), the intra-annual density fluctuation (IADF L) and latewood cells (LW), and (b) a detailed section of EW showing the measurements of lumen diameter (L) and quadruple cell wall thickness ($4w$, later divided by 4 to obtain single cell wall thickness). Image resolution is 0.68 µm pixel^{-1}.

the end calculated using a rectangular shape with a fixed width-to-length ratio ($f = 0.83$):

$$\rho_{\text{tracheid}} = 4\rho_{\text{cw}} \frac{((1+f)/2)(L/w)+1}{((L/w)+2)(f(L/w)+2)}. \quad (2)$$

A constant fraction ($f_{\text{live}} = 0.1$) of the ring representing resin duct canals and ray parenchyma cells, with a zero density (Panshin and De Zeeuw 1980), was further used to compute whole-wood density:

$$\rho = \rho_{\text{tracheid}} - f_{\text{live}}\langle\rho_{\text{tracheid}}\rangle, \quad (3)$$

where the brackets denote the mean over the entire ring. Although a value of up to 1.4 kg dm^{-3} is generally assumed for the cell wall density of dried wood, dry mass over green volume must be lower, owing to the absorption of water by the cell wall (Stamm 1964). We found that a green-state corrected value for ρ_{cw} of 1.0 kg dm^{-3} derived reasonable density values and was in agreement with previously published values (see review by Decoux et al. 2004).

Tracheid thickness-to-span ratio, an index for hydraulic safety to cell wall collapse (Hacke et al. 2001), was calculated as the ratio of the measured distance across the double cell wall between two adjoining tracheids and the tracheid diameter ($2w/L$). More specifically, the ratio was calculated for each tree ring as the mean value of $2w/L$ only for tracheids whose lumen diameter L is equal (within 2 μm) to the mean hydraulic diameter of the same ring (Hacke et al. 2001).

Theoretical specific conductivity (k_s, kg m^{-1} s^{-1} MPa^{-1}) was calculated for each ring using the modified Hagen–Poiseuille equation described by Tyree and Ewers (1991):

$$k_s = N\frac{\pi\rho_w}{128\eta}\langle L^4\rangle \quad (4)$$

where N (m^{-2}) is the tracheid density of the ring (computed from the average tracheid size), $\langle L^4\rangle$ denotes the mean of L^4 (m^4) over the entire ring, ρ_w is the fluid density (assumed to be 1 kg dm^{-3} or equal to that of water at 20 °C) and η is the fluid viscosity (assumed to be equal to that of water at 20 °C, i.e., 10^{-3} Pa s). Whole-ring hydraulic conductance (K, kg m^{-1} s^{-1} MPa^{-1}) was calculated as the product of k_s of each ring times the area (sapwood) of the ring.

Wood density profile measurements

Micro-density profiles were generated using the X-ray densitometry method developed by Polge (1966). From the same trees cored for anatomical image analysis, a 5-mm diameter core spanning bark to pith was extracted at breast height. Cores were divided into 2 mm sections, soaked in pentane to remove resins and then maintained at 12% humidity prior to X-ray exposure. Digitalized X-ray images were analysed and dated (in addition to manual cross-dating) using the Windendro software (Windendro, Regent Instruments Inc., Québec, Canada) at a 21.167 μm resolution.

Model description and parameterization

The Deleuze and Houllier (1998) model of cambial formation requires inputs of stand-level resource availability indices and temperature on a weekly time step. When the water availability index $R_{w,i}$ and air temperature $T_{air,i}$ of the ith week are above some pre-defined thresholds ($R_{w,min}$ and T_{min}, respectively), new cells are produced by the cambium and their number ($\Delta_{n,i}$), volume ($\Delta_{v,i}$) and mass ($\Delta_{m,i}$) are computed as follows:

$$\Delta_{n,i} = \Delta_{n,\max} \cdot [1 - e^{-\beta(T_{air,i} - T_{min})}] \quad (5a)$$

$$\Delta_{v,i} = \Delta_{v,\max} \cdot R_{w,i} \quad (5b)$$

$$\Delta_{m,i} = \Delta_{m,\max} \cdot [1 - e^{-\delta C_{pool,i}}] \quad (5c)$$

where $C_{pool,i}$ (kgC m^{-2} ground area) denotes the NSC pool size of the ith week, used here as the carbohydrate resource availability index, and other variables are model parameters described in Table 1. Wood density is then calculated as the ratio of $\Delta_{m,i}$ to $\Delta_{v,i}$ while ring width increment is computed from the product of $\Delta_{n,i}$ with $\Delta_{v,i}$ (Deleuze and Houllier 1998).

Note that, albeit in a crude way, this model also accounts for the influence of water availability on cambial division (cell number $\Delta_{n,i}$) as Eq. (5a) is only applied when $R_w > R_{w,min}$ and $T_{air,i} > T_{min}$.

Both $R_{w,i}$ and $C_{pool,i}$ were obtained from the MuSICA model (Ogée et al. 2003, 2009) using meteorological data from the site (Figure 2). In MuSICA, the NSC pool size is computed as the

Table 1. Summary of parameters needed for the density model and their values used in this study: minimum water availability index, $R_{w,min}$; minimum air temperature, T_{min}; maximum number of cells produced each week per radial file, $\Delta_{n,max}$; sensitivity of cell division to temperature, β; maximum volume of cells produced each week, $\Delta_{v,max}$; maximum increment mass produced each week, $\Delta_{m,max}$; cell thickening rate, δ; sensitivity of soil water availability index to soil water content, χ; critical soil water availability, $R_{w,crit}$; NSC pool turnover rate, k_{pool}.

Symbol (unit)	Value
$R_{w,min}$ (dimensionless)	0.5
T_{min} (°C)	3
$\Delta_{n,max}$ (week^{-1})	1.65
β (°C^{-1})	0.2
$\Delta_{v,max}$ (m^3 ha^{-1} week^{-1})	0.28
$\Delta_{m,max}$ (kgDW ha^{-1} week^{-1})	6400
δ (kgDW ha^{-1})$^{-1}$	0.1×10^{-4}
χ (dimensionless)	4
$R_{w,crit}$ (mm)	50
k_{pool} (year^{-1})	4

balance between leaf photosynthesis, maintenance respiration and whole-tree biomass synthesis, and the latter is taken proportional to the pool size $C_{pool,i}$ (source-driven hypothesis), with a constant rate coefficient k_{pool} (year^{-1}) (Ogée et al. 2009). At our sampling site, the MuSICA model is able to predict stand carbon and water fluxes at a half hourly time step in good agreement with the measured values obtained using the eddy-covariance technique (Ogée et al. 2003, 2009, Wingate et al. 2010). Deleuze and Houllier (1998) assumed that water availability was directly proportional to soil water content in the root zone. However, because of the high water table present at our site, bulk soil moisture levels were frequently above field capacity and so we preferred to characterize $R_{w,i}$ using a sigmoid function of the weekly soil water content in the root zone ($W_{soil,i}$), the latter being output by the MuSICA model:

$$R_{w,i} = 1 - \frac{1}{1 + (W_{soil,i}/W_{crit})^{\chi}}. \quad (6)$$

This function is linearly related to $W_{soil,i}$ up to about field capacity where it then saturates to unity. All parameter values were obtained iteratively by trial and error and are listed in Table 1. A simple model sensitivity analysis was also performed, varying one parameter at a time around its nominal value, in

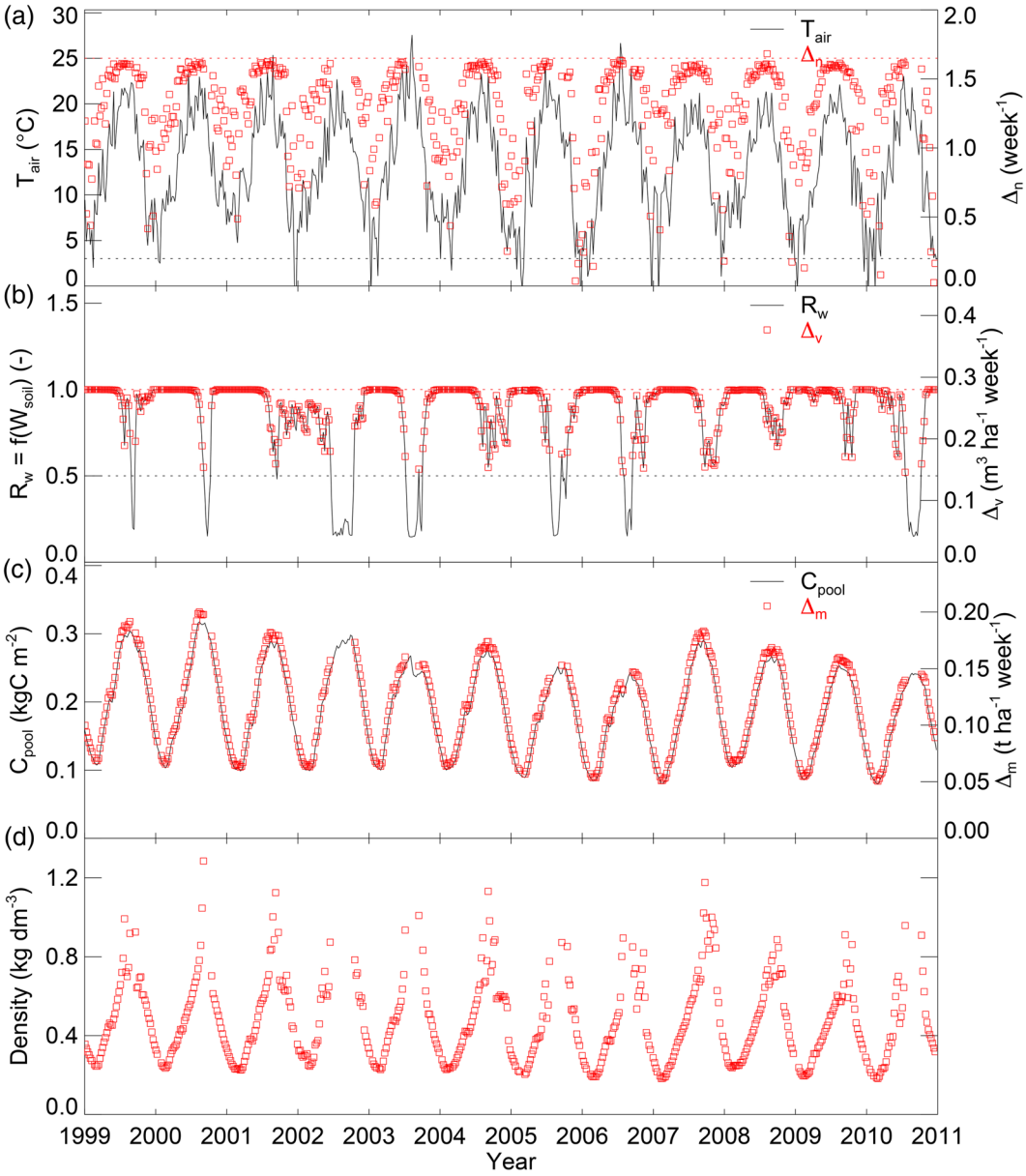

Figure 2. Time-series of the wood density model input and output variables: (a) mean weekly air temperature (T_{air}) and corresponding cell increment number (Δ_n), (b) plant water status (R_w) and corresponding cell volume increment (Δ_v), (c) plant NSC pool size (C_{pool}) and the corresponding cell mass increment (Δ_m) and (d) predicted wood density.

order to explore if multiple parameter sets could reproduce similar results. Results are shown in supplementary material (see Figure S3 available as Supplementary Data at *Tree Physiology* Online) and summarized below (Model evaluation).

Breakpoint analysis

To test the ability of the model to predict the occurrence and radial location of breakpoints in observed density profiles (i.e., the start- and end-points of density transitions and IADFs), and to compare these breakpoints with the changes in input variables, an analysis was carried out in the open-source statistical software R (R Core Team 2011) using the *bcp* package (Erdman and Emerson 2007). This package estimates the probability of an unknown partition (break point) between contiguous invariant blocks at any given location along a sequence. The algorithm builds upon the Barry and Hartigan (1993) product partition model for the standard change point problem using Markov Chain Monte Carlo with a default of 550 iterations (Erdman and Emerson 2007). Breakpoints were identified as the locations where the probability of a change was above a threshold of 55%. For IADF identification, breakpoints of higher than 0.55 posterior probability of a decrease in density defined the threshold for the IADF start boundary. Following the classification proposed by Campelo et al. (2007), the IADF was classified as type L if earlywood-like cells occurred within latewood, meaning that a decreasing density breakpoint was followed by a breakpoint for increasing density. If a decreasing density breakpoint was not followed by another breakpoint for increasing density, the IADF was classified as type L+ representing earlywood-like cells at the end of latewood, with a single breakpoint.

The location of the maximum probability for a breakpoint within each growth ring was ascertained, in order to compare patterns in observed and modelled profiles for probability of a change in density.

Results

Model evaluation

Model output of cell number per year was compared with the anatomical data (Figure 3). In general, observed cell numbers were at a maximum in 2001, 2007 and 2008 and at a minimum in 2002, 2005, 2006 and 2010. The model predicted a very similar inter-annual cell number pattern in most years, demonstrating the strong influence of air temperature on this parameter (Eq. (5a) and Figure 2a).

X-ray densitometry data suggested slightly larger rings (+20%) compared with anatomical observations, possibly because of the difference in azimuths between the two cores used for X-ray and anatomy observations. However, once corrected, both X-ray and anatomy data gave very similar inter-annual variations in ring width, in good agreement also with model predictions (Figure 3c). The strong similarity between cell

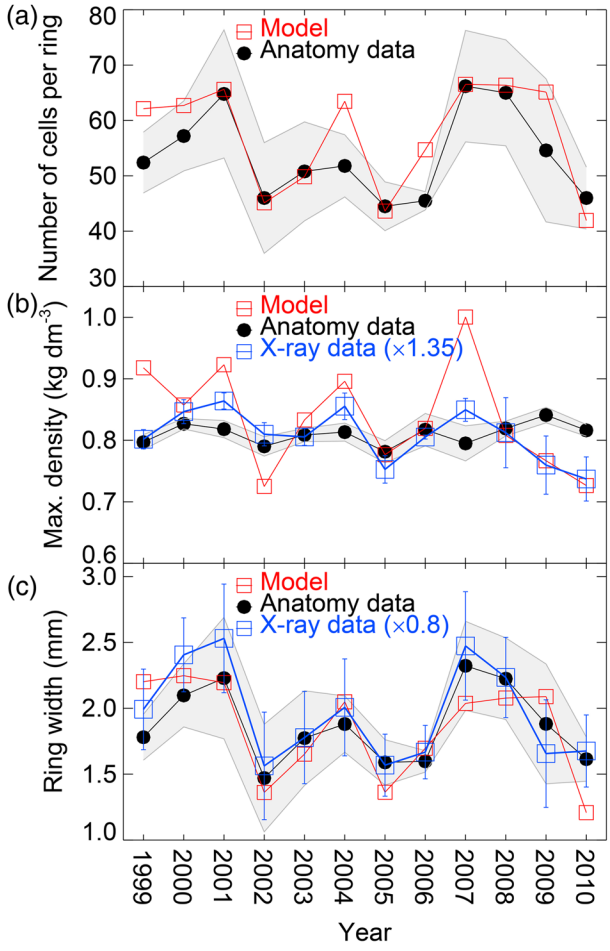

Figure 3. Yearly variations in (a) the number of cells per ring, (b) *MaxD* and (c) ring width from measured anatomical (black filled circles) and X-ray (blue open squares) data, compared with modelled output (red open squares). Anatomical measurements are means (±SE, indicated by the shaded area) over three radial files from anatomical images of annual growth rings of five trees. X-ray data are means from cores taken on the same five trees and were rescaled to match anatomical and model predictions (see text).

number and ring width variations also suggests that cell number is the main driver of ring width, both in the model and the data.

Modelled inter-annual variability in maximum wood density (75–95 percentiles) was also in good agreement with observations from either X-ray densitometry or anatomy data, although much larger than in the observations (Figure 3b). X-ray data predicted maximum density (*MaxD*) values ~35% lower than from the anatomy data, which can be partly attributed to the difference in spatial resolution of the two methods. However, once corrected the two data streams agreed very well, except in years 2009 and 2010, with X-ray densitometry indicating lower values that correspond with the model prediction.

Results shown in Figure 3 are based on whole-ring features only. Evaluating the model on intra-ring wood density profiles requires the phasing of model output with anatomical or X-ray data. Because the model also predicts ring width increment, we

first used the within-ring distance as a phasing variable (Figure 4). As for *MaxD* in Figure 3b, intra-ring density values estimated by X-ray densitometry were lower (by ~35%) compared with values estimated through image analysis. However, the phasing of the radial profiles was similar between the two data streams. In comparison, density profiles predicted by the model usually exhibited greater amplitude than those obtained via image analysis or X-ray densitometry (e.g., in 2007), and the *MaxD* peak tended to appear a bit too early (e.g., in 2002 or 2003).

Because the model and the anatomical data showed a very good agreement on the number of cells per growth rings (Figure 3b) we also tried using the cell number within a growth ring as a temporal reference to date the spatial information obtained from the image analysis. For trees and growth rings where the observed number of cells was particularly well predicted by the model (e.g., tree 6138 on year 2001) wood density from the image analysis could then be directly related to

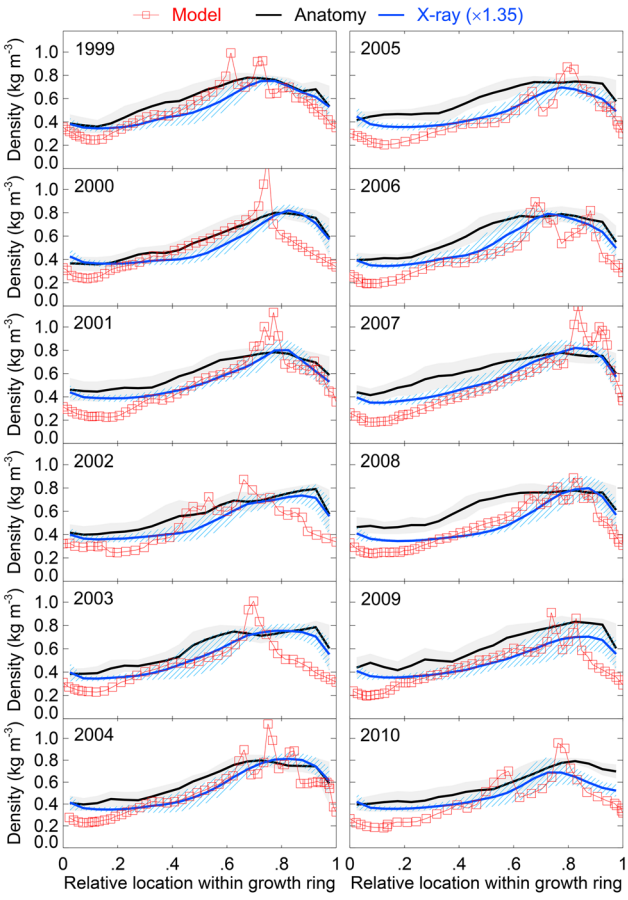

Figure 4. Radial series of intra-annual density profiles generated using anatomical (black lines) and X-ray densitometry (blue lines) measurements compared with modelled density profiles (red open squares) for each growth ring. Anatomical measurements are means (±SE, indicated by the shaded area) over three radial files from anatomical images of annual growth rings of five trees. X-ray data are means (±SE, indicated by the hatched area) from cores taken on the same five trees and was rescaled to match anatomical and model predictions (see text).

air temperature, water or NSC availability on a weekly time step (Figure 5). Bayesian breakpoint analysis was additionally applied to model input variables and modelled and observed density profiles using a cut-off probability of 75%. A single definable breakpoint emerged at position 40 in the anatomy data, whereas two peaks were detected in the modelled density profile (Figure 5a) that coincided with rapid changes and one breakpoint in soil water availability (Figure 5b). The link with changes in air temperature or NSC availability was less pronounced (Figure 5c and d).

Phasing the anatomy data using cell number rather than distance within the ring allowed a direct comparison with weekly model output and confirmed that the agreement between measured and modelled density values was satisfying, as shown here for trees 6138 and 6119 and year 2001 (Figure 6a). There was a strong negative relationship between modelled wood density and available soil water ($R^2 = 0.93$) (Figure 6b). Although this relationship was linear over a wide range of density values, above field capacity ($R_w = 1$), variability in modelled density was apparent. The observed density also exhibited some negative relationship with available soil moisture but the linear correlation was weak (data not shown).

Inter-annual variability in xylem anatomy and hydraulic efficiency

Image analysis revealed that variations in lumen diameter were higher than variations in cell wall thickness throughout the growing season (Figure 7a). This resulted in strongly significant ($P < 0.001$) linear regressions between density values calculated using Eq. (3) and lumen diameter (Figure 7b). Extrapolating the linear regression obtained on latewood cells to a lumen diameter of zero leads to a density value of 0.95 kg dm^{-3}, i.e., lower than the cell wall density value of $\rho_{cw} = 1.0$ kg dm^{-3} used in Eq. (2). The difference is caused by the fraction of the ring $f_{live} = 0.1$ with a zero density.

The anatomy data also revealed that a trade-off existed between hydraulic safety (represented by the cell wall thickness-to-span ratio $2w/L$ of the most conducting tracheids) and hydraulic efficiency (represented by the mean specific hydraulic conductivity k_s of all tracheids within a ring) (Figure 8). However, in 2002 (a very dry year; Figure 1), the anatomical data showed an unusually low k_s value that should have corresponded to very high thickness-to-span ratios, not observed in the anatomical images. This probably shows a plastic limit in tracheid geometry during very dry years. These inter-annual variations in tracheid hydraulic efficiency (k_s) did not always translate into similar changes in whole-ring hydraulic conductance (K) because of the modulation caused by the sapwood area allocated to each ring (Figure 9). In fact, whole-ring sapwood area seemed a better indicator of dry years (2002, 2003, 2005, 2006, 2010; Figure 1) than k_s, which exhibited high values during some of these dry years (e.g., 2009 or 2010) (Figure 9). This disparity between hydraulic conductivity at the scale of

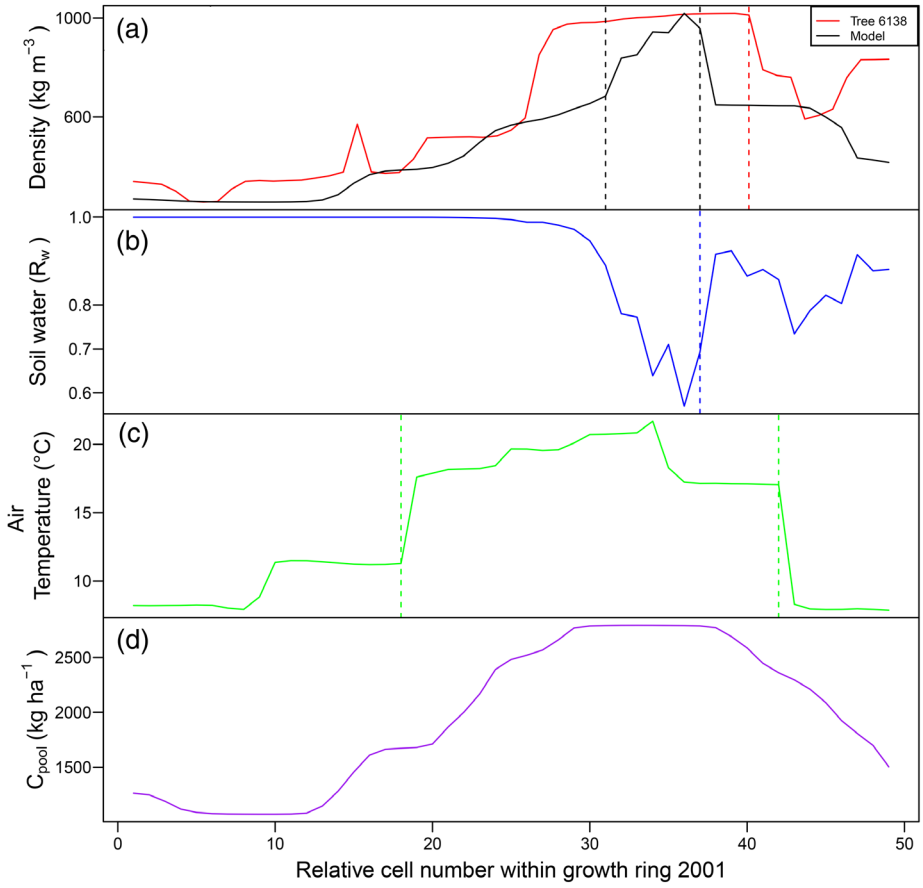

Figure 5. Bayesian break point analyses for (a) observed and modelled density profiles, (b) plant water availability R_w, (c) air temperature and (d) NSC pool size C_{pool} for tree 6138 and year 2001. The time-series break-point analysis was performed using the bcp package in R language, with the default (550) number of iterations. Intra-annual density fluctuation boundary positions for model and observed density profiles correspond to a 50% probability of a change.

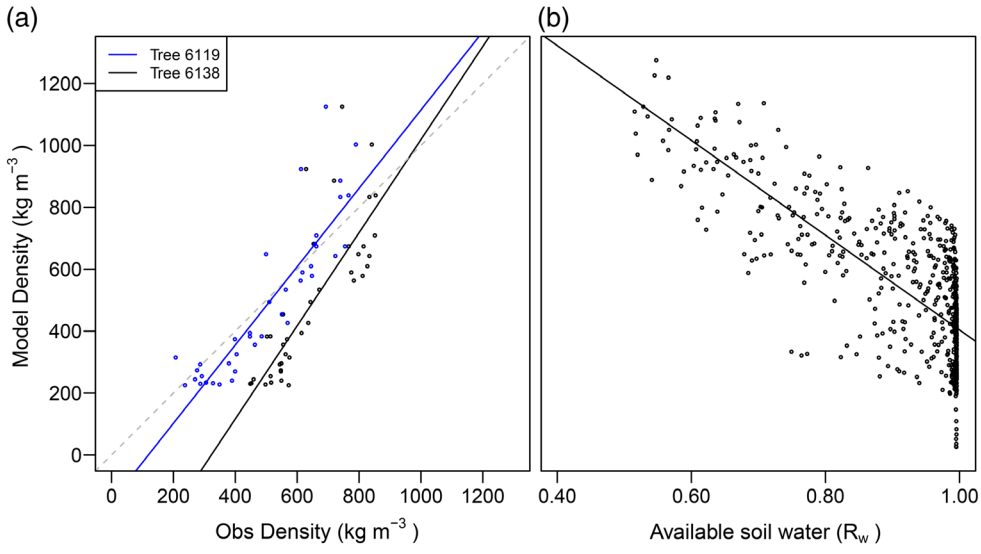

Figure 6. Predicted wood density (kg m^{-3}) plotted against (a) observed wood density in the 2001 growth ring of trees 6138 and 6119 and (b) modelled plant water status for all growth rings. Trees 6138 and 6119 in year 2001 were selected for analysis with identical tracheid number (55 cells) and phased with the tracheid number predicted by the model (64 cells).

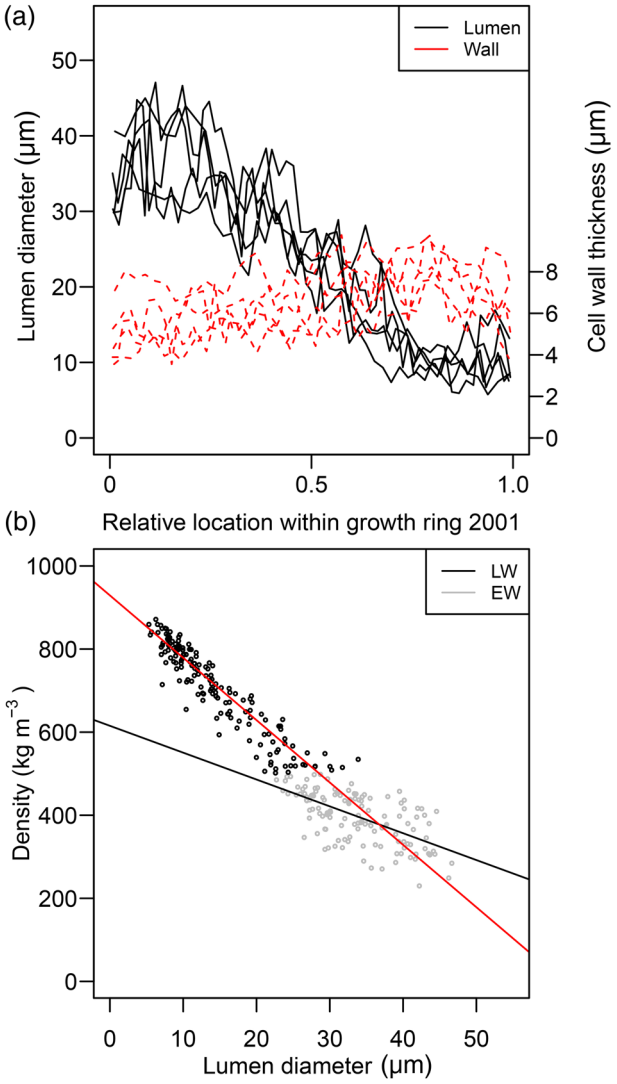

Figure 7. Variations in lumen diameter and cell wall thickness within the 2001 growth ring (a) and relationship between lumen diameter and wood density based on anatomical measurements (b) for the five studied trees. In (b) linear regressions were fitted separately for latewood (black circles) and earlywood (grey circles) cells.

tracheids and the entire ring was confirmed by the lack of any significant difference between the mean number of cells in rings with and without IADFs.

Intra-annual density fluctuations

Based on the five sampled trees used for anatomy data, L-type IADFs seemed frequent at our site, occurring in all years with a relative observed frequency above 0.6, except in 2002, 2003, 2007 and 2008 (Table 2). L+-type IADFs identified in the middle of the latewood typically occurred with a lower relative observed frequency than L-type ones, except in 2002 and 2003, and also 2007, where they appeared with higher frequency (up to 0.7 in 2002).

For most years the model predicted the dominant IADF type according to the relative observed frequency, except in 2003

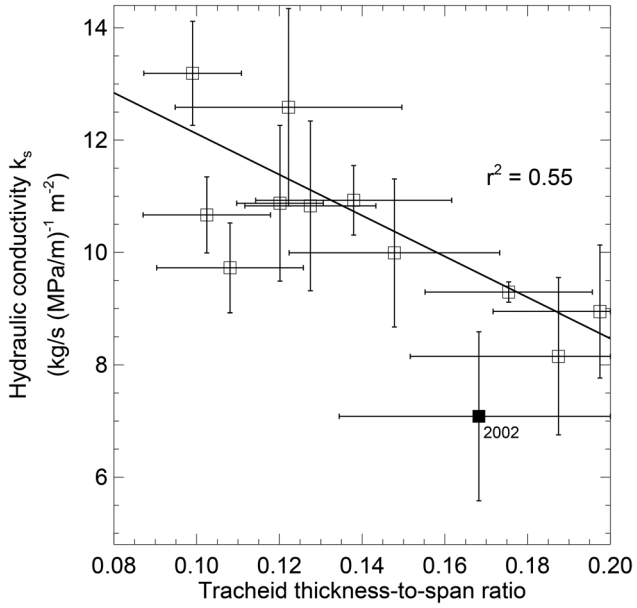

Figure 8. Relationship between mean theoretical tracheid hydraulic conductivity and mean thickness-to-span ratio for each annual ring. Year 2002 is highlighted, as it seems to fall out of the linear, negative trade-off observed for the other years (solid line).

and 2007 where the model predicted L-type IADF while L+-type IADFs were more frequently observed in the data. Also the model tended to predict more rings with both L- and L+-type IADFs than suggested by the data.

The location within the ring of the maximum probability for a change in density also differed between anatomical, X-ray and modelled density profiles (see Figure S1 available as Supplementary Data at *Tree Physiology* Online). For all years, density profiles derived from anatomical images exhibited a maximum probability of a change in density earlier in the ring than for both X-ray and model data. Relative ring locations of the maximum probability of a change in model density followed more closely the relative ring locations obtained from X-ray density (see Figure S1 available as Supplementary Data at *Tree Physiology* Online).

Discussion

Model evaluation

Overall, X-ray densitometry indicated lower density values than those calculated from the lumen/cell wall ratios observed in light microscope images. Overestimation of density by anatomical methodology may account for some of the disparity (Decoux et al. 2004), although another study on *P. pinaster* (Sánchez-Vargas et al. 2007) reported *MaxD* values obtained by X-ray densitometry of 0.9 kg dm^{-3}, i.e., much higher than the 0.6 kg dm^{-3} value typically found in this study. Model density variations were typically spanning the same range, however they showed greater amplitude than either image analysis or X-ray

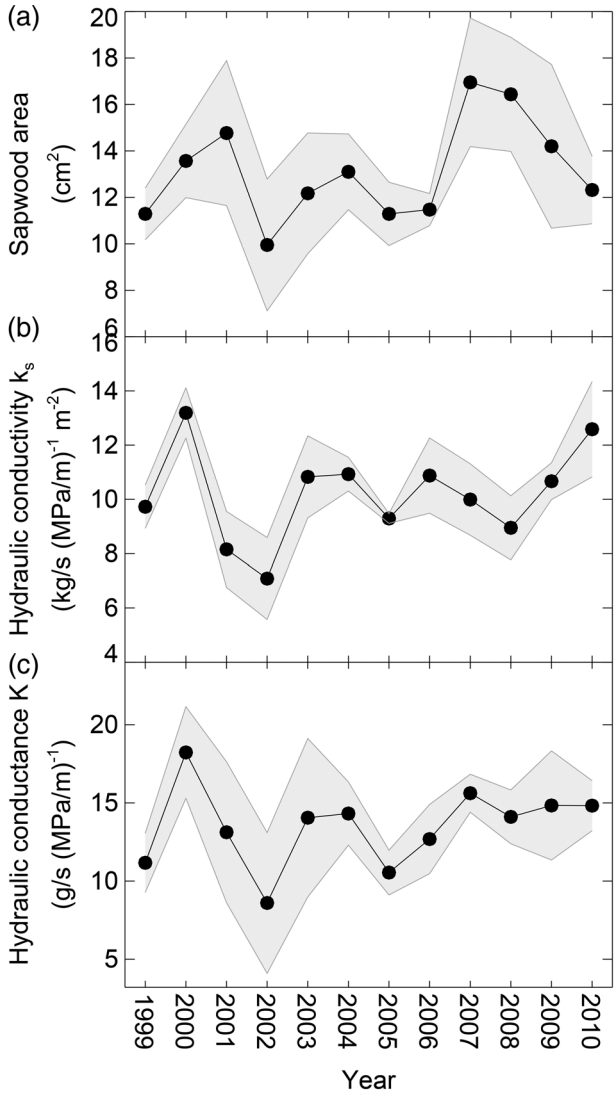

Figure 9. Whole-ring variations of (a) sapwood area, (b) theoretical specific conductivity and (c) theoretical hydraulic conductance, calculated from anatomical images.

densitometry, suggesting model oversensitivity to one or more driving variables and indicating the requirement of a buffering effect in the cambial response to environmental conditions or additional constraints not accounted for in the model.

The model sensitivity analysis (see Figure S3 available as Supplementary Data at *Tree Physiology* Online) also indicated possible over-parameterization of the model equations. For example parameters for maximum cell number ($\Delta_{n,max}$) and sensitivity of cell division to temperature (β) are strongly correlated because they have the same effect on the number of cells (*N*) and tree-ring width (*TRW*), and no effect on *MaxD*. Thus, new parameter sets could be defined, which produce nearly the same results. For example, if the minimum temperature value (3 °C) is increased to 7 °C concurrently with β from 0.2 to 0.6, then *MaxD* remains unchanged (and also all the density profiles in general), and *TRW* and *N* also remain almost identical (see Figure S4 available as Supplementary Data at *Tree Physiology* Online).

Table 2. Relative frequency and type of IADFs for each growth ring (1999–2010) as observed in image analysis, X-ray densitometry or predicted from the density model. Relative observed frequency was calculated using the 10 tree cores (5 for image analysis and 5 for X-ray densitometry). Intra-annual density fluctuations were detected in density profiles containing breakpoints with a 0.55 probability of a change identified by the bcp() package. L-type IADFs correspond to decreasing density breakpoints at the end of latewood, not followed by a breakpoint for increasing density, while L+-type IADFs correspond to decreasing density breakpoints in the centre of latewood, followed by a breakpoint for increasing density. No IADFs correspond to the situation when a breakpoint for increasing density is not followed by a breakpoint for decreasing density.

Year	L+-type IADF (relative observed frequency)	L-type IADF (relative observed frequency)	Model IADF type
1999	0	0.7	L+, L
2000	0.1	0.8	L
2001	0.1	1	L
2002	0.7	0.2	L+, L
2003	0.4	0.3	L
2004	0.1	0.6	L+, L
2005	0	0.6	L
2006	0	1	L+, L
2007	0.5	0.1	L
2008	0.2	0.4	L+[1], L
2009	0.1	0.6	L+, L
2010	0.1	0.8	L+, L

[1]Minor IADFs.

Cell production

Cambium activity did not always respond to late season water availability. Recovery from the 2002 drought was not observed in tree rings that did not form any IADFs, despite the occurrence of autumn rains. The model also appeared to overreact to the transient change in water availability in 2007. Wingate et al. (2010) reported increased transpiration rates in response to a sudden recharge of soil water in late August of 2007. However, the cambium did not appear to react by increasing tracheid radial diameter in response to the recharged soil water, indicated by the absence of an IADF observed in the latewood of 2007. This possibly indicates that cambial responses are buffered from rapid changes in environmental signals, at least in the latewood, and that a sustained increase in turgor is necessary to invoke detectable changes in wood density.

Intra-annual density fluctuations

Most of the IADFs were found in the latewood, corroborating other works identifying latewood IADFs as the most common type in *P. pinaster* (Vieira et al. 2010, Rozas et al. 2011). Upon examining these intra-ring features, the model appeared to function as an effective link between variations in environmental conditions and wood density variation in some years more than others. Based on the threshold of a relative frequency >0.5, the

model correctly predicted L-type IADFs (Table 2). For example, in 2001, modelled density showed a better relationship with observed wood density than with water availability data alone and exhibited similar points of change as the observed density profile (Figures 4 and 5). Comparisons of the location of the maximum probability of a change in density between anatomical, X-ray and model density indicate that anatomically identified IADFs typically do not reflect the maximum probability of a change in density within a ring, which instead is more likely to be attributable to the earlywood/latewood transition. However, the X-ray and model position of maximum probability of a change in density occurred later in the ring and potentially corresponded to the latewood IADF location.

Wood density is usually considered to be an adaptive trait under severe drought, although not necessarily correlated with resistance to embolism (Jacobsen et al. 2005, Meinzer et al. 2008) or percentage of leaf area desiccated (Hoffmann et al. 2011). Some studies have argued that latewood cells, which constitute the main driver of ring density in conifers, are more sensitive to losing water under drought conditions, which may provide a buffering effect through an increase in hydraulic capacitance without much alteration to the overall hydraulic conductivity (Domec and Gartner 2002*b*, Domec et al. 2009). In support of this hypothesis, Douglas fir trees surviving in France after the 2003 European drought exhibited a higher latewood density and an increased proportion of latewood compared with neighbouring trees that died shortly after the drought event (Martinez-Meier et al. 2008). However, other studies unexpectedly report that thick latewood and high wood density are associated with higher drought-induced mortality rates (Hoffmann et al. 2011, Kukowski et al. 2013). Rigling et al. (2002) found a lower proportion of latewood and a concomitant increase in IADF frequency in *Pinus sylvestris* growing on drier sites. Thus, an exact physiological process involved in the formation of latewood IADFs when favourable conditions return after summer is not clearly posited. However, the question of whether the resumption of cambial activity after drought holds adaptive significance has been raised for *P. pinaster*. Campelo et al. (2013) and Nabais et al. (2014) demonstrate that, though the functional mechanism remains elusive, IADF formation in *P. pinaster* exhibits a strong positive correlation with precipitation following summer drought.

Water availability: a key driver of intra-annual density patterns?

Changes in tracheid features could potentially impact stem water conductive and storage capacity. The observed negative tradeoff between hydraulic safety and efficiency at the cellular level (Figure 8) was expected. Thus, if IADFs have a conductive role, then they will increase hydraulic safety during drought periods. However, the hydraulic conductance of any growth ring (K) also depends on the total number of cells produced (i.e., the ring sapwood area) rather than their specific conductivity alone (Figure 9). However, there may remain a potential effect of hydraulic capacitance enabled by earlywood-like cells within latewood, since IADFs would store water that could be used by trees during drought periods (Domec and Gartner 2002*b*, Deslauriers et al. 2008).

The model's ability to accurately estimate total cell numbers within the observed range was encouraging, although cell division seemed to have a higher capacity for recovery after drought than predicted by the model, leading to an underestimate in cell number for 2010 (Figure 5). Anatomical data provided an opportunity to test the mechanistic assumptions of the model. For example, the different stages in xylem differentiation are assumed to be delineated (Eqs (5a–c)), while in reality they are intimately connected. This decoupling between carbon-, water- and temperature-limited processes may account for some of the model error. Cambial turgor pressure is determined both by xylem water potential and phloem sugar concentration gradients, indicating that the model assumption of a linear relationship with soil water is oversimplified (Hölttä et al. 2010). In addition, latewood tracheids tend to undergo secondary cell wall (S2) thickening over a prolonged period, thereby also contributing to an increased cell wall thickness (Kozlowski 1971, Plomion et al. 2001, Vaganov et al. 2006). Nevertheless, it appears that the model's ability to predict cell volume was the key output explaining differences between modelled and observed density. Thus, future efforts should be focused on improving the representation of turgor dynamics in MuSICA by coupling water and carbon more intimately as shown in other models (Drew et al. 2010, Hölttä et al. 2010).

Prediction of cell volume was highly sensitive to cell enlargement rate, which may implicate a genetic component in cell expansion. Cell enlargement rate is proportional to soil moisture in the model, yet biological constraints affect the extent of dependence of the cambial environment on the soil environment. Xylem ontogeny is thought to be regulated by auxin concentration along morphogenic gradients (Kramer 2001, Uggla et al. 2001, Schrader et al. 2003, Drew et al. 2010). Welsh (2006) found that increasing the concentration of auxin in media for stem organ culture drastically increased radial tracheid diameter. Meanwhile, reduced xylem lumen in trees exposed to water deficit is also associated with a reduction in free indole-3-acetic acid (IAA) that limits cell expansion (Popko et al. 2010). Hormonal signals, along with coupled carbon–water fluxes, may thus represent key differences between the external and cambial environment, which may lead to a re-interpretation of changes in water availability. However, disentangling the impact of turgor pressure from cell wall sensitivity is problematic. Polar auxin transport is linked to seasonal changes in shoot photosynthesis, which in turn are affected by water availability. Whether cells in cambium react first to a rapid increase in xylem turgor pressure caused by a rain event, or

increased IAA and sugars caused by higher photosynthetic activity, is not clear. There is a direct impact of water. However, the temporally lagged metabolic signalling of increased whole-tree water status may also have an intrinsic role in shaping xylem development. This cannot be accounted for in the model as it is currently formulated.

Another factor to consider when comparing model and observed wood density is the sampled tree height. This study evaluated model performance based on mature base wood, yet the cambial age gradient declines vertically. Corresponding changes are reported in gene expression of developing xylem tissue in *P. pinaster*, with cambial activity in the crown exhibiting higher rates of cell division and expansion than the base, where genes linked to cell wall thickening were upregulated (Paiva et al. 2008). Similarly, in *Pinus radiata*, re-modelling of the xylem transcriptome is found between age classes, as well as between early and late season growth (Li et al. 2010). Furthermore, stem size mediates the effect of climatic conditions on cambial activity in an even-aged stand of *P. pinaster* in the Mediterranean climate in Portugal, reflecting the need to stratify by size class in order to increase sensitivity to the IADF signal (Campelo et al. 2013). Hence, the response to water availability in terms of IADF formation may have been more pronounced in crown wood with younger cambial tissue or fast-growing trees of the larger size class. This effect could be accounted for by model parameters that could be size- and height-adjusted, such as xylem water potential.

Conclusion

In *P. pinaster*, IADFs often form in the latewood and biophysical modelling was able to predict this growth response, along with similar rates of cell production. Although water availability appeared to be the key driver of wood density variation, the main flaw in model prediction was an oversensitivity to water availability. A buffering effect between the environmental variation and cambial response seems to be necessary to reconcile model density and data. Whether this could be achieved through the coupling of carbon–water fluxes to derive cambial turgor pressure or by integrating hormonal control of xylem development now needs to be explored.

Despite these constraints, the linking of a simple cambial model to a mechanistic model of resource availability enabled reasonable predictions of intra-annual wood density features and growth ring cell number. MuSICA is currently being parameterized for several other FluxNet sites, representing forest stands in both temperature-limited (Varrio, Finland) and water-limited (Yatir, Israel) conditions. Hence, future work will be able to compare model predictions of radial growth trends across a broader environmental gradient and provide a framework for investigating tree growth responses at a more general scale.

Supplementary data

Supplementary data for this article are available at *Tree Physiology* Online.

Acknowledgments

We would like to thank Frédéric Lagane from the Genobois platform at INRA Pierroton for performing very promptly the X-ray wood density analysis on our wood samples. Many thanks to Michel le Hénaff for lending us his microscope and video camera system. The authors wish to thank the communicating Editor and two anonymous reviewers for their suggestions and comments that helped to improve the original version of the paper.

Conflict of interest

None declared.

Funding

This work was funded by the ANR project MIST (ANR-07-BLN-0131) awarded to J.O. and the INRA ACCAF meta-programme. J.-C.D. was also partly supported by the DOE-BER Terrestrial Ecosystem Sciences program (grant 11-ER65189) and by the USP-COFECUB grant (UcSv 134/12, 2012–2015).

References

Abe H, Nakai T (1999) Effect of the water status within a tree on tracheid morphogenesis in *Cryptomeria japonica* D. Don. Trees 14:124–129.

Abe H, Nakai T, Utsumi Y, Kagawa A (2003) Temporal water deficit and wood formation in *Cryptomeria japonica*. Tree Physiol 23:859–863.

Barry D, Hartigan JA (1993) A Bayesian analysis for change point problems. J Am Stat Assoc 88:309–319.

Battipaglia G, De Micco V, Brand WA, Linke P, Aronne G, Saurer M, Cherubini P (2010) Variations of vessel diameter and $\delta^{13}C$ in false rings of *Arbutus unedo* L. reflect different environmental conditions. New Phytol 188:1099–1112.

Bouriaud O, Leban J-M, Bert D, Deleuze C (2005) Intra-annual variations in climate influence growth and wood density of Norway spruce. Tree Physiol 25:651–660.

Campelo F, Nabais C, Freitas H, Gutiérrez E (2007) Climatic significance of tree-ring width and intra-annual density fluctuations in *Pinus pinea* from a dry Mediterranean area in Portugal. Ann For Sci 64:229–238.

Campelo F, Vieira J, Nabais C (2013) Tree-ring growth and intra-annual density fluctuations of *Pinus pinaster* responses to climate: does size matter? Trees 27:763–772.

Choat B, Cobb AR, Jansen S (2008) Structure and function of bordered pits: new discoveries and impacts on whole-plant hydraulic function. New Phytol 177:608–626.

Decoux V, Varcin E, Leban JM (2004) Relationships between the intra-ring wood density assessed by X-ray densitometry and optical anatomical measurements in conifers. Consequences for the cell wall apparent density determination. Ann For Sci 61:251–262.

Deleuze C, Houllier F (1998) A simple process-based xylem growth model for describing wood microdensitometric profiles. J Theor Biol 193:99–113.

Delzon S, Douthe C, Sala A, Cochard H (2010) Mechanism of water-stress induced cavitation in conifers: bordered pit structure and function support the hypothesis of seal capillary-seeding. Plant Cell Environ 33:2101–2111.

De Micco V, Saurer M, Aronne G, Tognetti R, Cherubini P (2007) Variations of wood anatomy and δ13C within-tree rings of coastal *Pinus pinaster* showing intra-annual density fluctuations. IAWA J 28:61–74.

Deslauriers A, Rossi S, Anfodillo T, Saracino A (2008) Cambial phenology, wood formation and temperature thresholds in two contrasting years at high altitude in southern Italy. Tree Physiol 28:863–871.

Domec J-C, Gartner BL (2002*a*) How do water transport and water storage differ in coniferous earlywood and latewood? J Exp Bot 51:2369–2379.

Domec J-C, Gartner BL (2002*b*) Age- and position-related changes in hydraulic versus mechanical dysfunction of xylem: inferring the design criteria for Douglas-fir wood structure. Tree Physiol 22:91–104.

Domec J-C, Meinzer FC, Gartner BL, Woodruff D (2006) Transpiration-induced axial and radial tension gradients in trunks of Douglas-fir trees. Tree Physiol 26:275–284.

Domec J-C, Warren JM, Meinzer FC, Lachenbruch B (2009) Safety factors for xylem failure by implosion and air-seeding within roots, trunks and branches of young and old conifer trees. IAWA J 30:101–120.

Domec J-C, Ogée J, Noormets A, Jouangy J, Gavazzi M, Treasure E, Sun G, McNulty SG, King JS (2012) Interactive effects of nocturnal transpiration and climate change on the root hydraulic redistribution and carbon and water budgets of southern United States pine plantations. Tree Physiol 32:707–723.

Drew DM, Downes GM, Battaglia M (2010) CAMBIUM, a process-based model of daily xylem development in Eucalyptus. J Theor Biol 264:395–406.

Erdman C, Emerson JW (2007) bcp: an R package for performing a Bayesian analysis of change point problems. J Stat Softw 23:1–13. http://www.jstatsoft.org/v23/i03/.

Fritts HC (1966) Growth-rings of trees: their correlation with climate. Science 154:973–979.

Fritts HC (2001) Tree rings and climate. The Blackburn Press, London.

Hacke UG, Sperry JS, Pockman WT, Davis SD, McCulloh KA (2001) Trends in wood density and structure are linked to prevention of xylem implosion by negative pressure. Oecologia 126:457–461.

Hoffmann WA, Marchin RM, Abit P, Lau OL (2011) Hydraulic failure and tree dieback are associated with high wood density in a temperate forest under extreme drought. Glob Change Biol 17:2731–2742.

Hölttä T, Makinen H, Nojd P, Makela A, Nikinmaa E (2010) A physiological model of softwood cambial growth. Tree Physiol 30:1235–1252.

Jacobsen AL, Ewers FW, Pratt RB, Paddock WA, Davis SD (2005) Do xylem fibers affect vessel cavitation resistance? Plant Physiol 139:546–556.

Kozlowski TT (1971) Growth and development of trees: cambial growth, root growth, and reproductive growth. Academic Press, London.

Kramer EM (2001) A mathematical model of auxin-mediated radial growth in trees. J Theor Biol 208:387–397.

Kukowski KR, Schwinning S, Schwartz BF (2013) Hydraulic responses to extreme drought conditions in three co-dominant tree species in shallow soil over bedrock. Oecologia 171:819–830.

Larson PR (1994) The vascular cambium. Development and structure. Springer, Berlin, Heidelberg.

Li X, Wu HX, Southerton SG (2010) Seasonal reorganization of the xylem transcriptome at different tree ages reveals novel insights into wood formation in *Pinus radiata*. BMC Evol Biol 10:764–776.

Lockhart JA (1965) An analysis of irreversible plant cell elongation. J Theor Biol 8:264–275.

Martinez-Meier A, Sanchez L, Pastorino M, Gallo L, Rozenberg P (2008) What is hot in tree rings? The wood density of surviving Douglas-firs to the 2003 drought and heat wave. For Ecol Manag 256:837–843.

Meinzer FC, Campanello PI, Domec JC, Gatti MG, Goldstein G, Villalobos-Vega R, Woodruff DR (2008) Constraints on physiological function associated with branch architecture and wood density in tropical forest trees. Tree Physiol 28:1609–1617.

Nabais C, Campelo F, Vieira J, Cherubini P (2014) Climatic signals of tree-ring width and intra-annual density fluctuations in *Pinus pinaster* and *Pinus pinea* along a latitudinal gradient in Portugal. Forestry 87:598–605.

Ogée J, Brunet Y, Loustau D, Berbigier P, Delzon S (2003) MuSICA, a CO_2, water and energy multilayer, multileaf pine forest model: evaluation from hourly to yearly time scales and sensitivity analysis. Glob Change Biol 9:697–717.

Ogée J, Barbour MM, Wingate L et al. (2009) A single-substrate model to interpret intra-annual stable isotope signals in tree-ring cellulose. Plant Cell Environ 32:1071–1090.

Paiva JAP, Garcés M, Alves A et al. (2008) Molecular and phenotypic profiling from the base to the crown in maritime pine wood-forming tissue. New Phytol 178:283–301.

Panshin AJ, De Zeeuw C (1980) Textbook of wood technology, 4th edn. McGraw-Hill, New York.

Park Y-I, Dallaire G, Morin H (2006) A method for multiple intra-ring demarcation of coniferous trees. Ann For Sci 63:9–14.

Pittermann J, Sperry JS, Wheeler JK, Hacke UG, Sikkema EH (2006) Mechanical reinforcement of tracheids compromises the hydraulic efficiency of conifer xylem. Plant Cell Environ 29:1618–1628.

Plomion C, Leprovost G, Stokes A (2001) Wood formation in trees. Plant Physiol 127:1513–1523.

Polge H (1966) Etablissement des courbes de variations de la densité du bois par exploration densitométrique de radiographies d'échantillons prélevés à la tarière sur des arbres vivants. Application dans les domaines technologiques et physiologiques. Thèse de doctorat, Université de Nancy, Nancy, France.

Popko J, Hänsch R, Mendel R-R, Polle A, Teichmann T (2010) The role of abscisic acid and auxin in the response of poplar to abiotic stress. Plant Biol 12:242–258.

R Core Team (2011) R: a language and environment for statistical computing. R Foundation for Statistical Computing, Vienna, Austria. http://www.R-project.org/.

Rigling A, Waldner PO, Forster T, Bräker OU, Pouttu A (2001) Ecological interpretation of tree-ring width and intraannual density fluctuations in *Pinus sylvestris* on dry sites in the central Alps and Siberia. Can J For Res 31:18–31.

Rigling A, Bräker O, Schneiter G, Schweingruber F (2002) Intra-annual tree-ring parameters indicating differences in drought stress of *Pinus sylvestris* forests within the Erico-Pinion in the Valais (Switzerland). Plant Ecol 163:105–121.

Rozas V, García-González I, Zas R (2011) Climatic control of intra-annual wood density fluctuations of *Pinus pinaster* in NW Spain. Trees 25:443–453.

Sánchez-Vargas N, Sánchez L, Rozenberg P (2007) Plastic and adaptive response to weather events: a pilot study in a maritime pine tree ring. Can J For Res 37:2090–2095.

Savidge RA (2001) Intrinsic regulation of cambial growth. J Plant Growth Regul 20:52–77.

Schrader J, Baba K, May ST, Palme K, Bennett M, Bhalerao RP, Sandberg G (2003) Polar auxin transport in the wood-forming tissues of hybrid aspen is under simultaneous control of developmental and environmental signals. Proc Natl Acad Sci USA 100:10096–10101.

Schweingruber FH (1988) Tree rings: basics and applications of dendrochronology. D. Reidel Publishing Company, Dordrecht, The Netherlands.

Sperry JS, Meinzer FC, McCulloh KA (2008) Safety and efficiency conflicts in hydraulic architecture: scaling from tissues to trees. Plant Cell Environ 31:632–645.

Stamm AJ (1964) Wood and cellulose science. Ronald Press, New York.

Tyree MT, Ewers FW (1991) The hydraulic architecture of trees and other woody plants. New Phytol 119:345–360.

Tyree MT, Sperry JS (1989) Vulnerability of xylem to cavitation and embolism. Annu Rev Plant Physiol Plant Mol Biol 40:19–38.

Tyree MT, Zimmermann MH (2002) Xylem structure and the ascent of sap. Springer, Heidelberg, Germany.

Uggla C, Magel E, Moritz T, Sundberg B (2001) Function and dynamics of auxin and carbohydrates during earlywood/latewood transition in Scots pine. Plant Physiol 125:2029–2039.

Vaganov EA, Hughes MK, Shashkin EA (2006) Growth dynamics of conifer tree rings: images of past and future environments. Springer, Heidelberg.

Vieira J, Campelo F, Nabais C (2010) Intra-annual density fluctuations of *Pinus pinaster* are a record of climatic changes in the western Mediterranean region. Can J For Res 40:1567–1575.

Welsh S (2006) Hormonal control of wood formation in radiata pine. Ph.D. dissertation. University of Canterbury, Christchurch, New Zealand.

Wimmer R, Strumia G, Holawe F (2000) Use of false rings in Austrian pine to reconstruct early growing season precipitation. Can J For Res 30:1691–1697.

Wingate L, Ogée J, Burlett R, Bosc A, Devaux M, Grace J, Loustau D, Gessler A (2010) Photosynthetic carbon isotope discrimination and its relationship to the carbon isotope signals of stem, soil and ecosystem respiration. New Phytol 188:576–589.

Zweifel R, Zeugin F, Zimmermann L, Newbery DM (2006) Intra-annual radial growth and water relations of trees: implications towards a growth mechanism. J Exp Bot 57:1445–1459.